Microstructural change in high temperature heat-affected zone of low carbon weldable “13 %Cr” martensitic stainless steels

D. Carrouge, Pr. H.K.D.H Bhadeshia, Department of Materials science and Metallurgy, University of Cambridge and Dr. P.Woollin, TWI Ltd. Granta park UK

Abstract

The microstructures that develop in the high temperature heat-affected zone[1] (HT-HAZ) of single pass T.I.G. welded plates of two different low carbon martensitic stainless steels have been investigated using optical microscopy and energy dispersive X-ray microanalysis. Particular attention has been given to the presence of retained δ-ferrite in the HT-HAZ. The region containing δ-ferrite was found to be larger in the HAZ of the highest alloyed steel. Evidence of former Widmanstätten austenite structure was found in the weld metal and in the grain coarsened heat-affected zone (CG-HAZ) of the highest alloyed steel.

Introduction

Low carbon and modified[2] low carbon “13 %Cr” martensitic stainless steels have started to be employed in different parts of the world as alternative materials to duplex stainless steels for multiple purpose use in the oil and gas industries. The unique combination of comparatively low price, high strength, corrosion resistance and weldability render these alloys extremely attractive. The new steels have recently been introduced and as yet no field failures of the welded materials have been reported. If failures occur they are likely in the heat-affected zones due to the microstructural changes that take place in these areas during welding. So far, little attention has been paid to understanding the microstructural evolution that takes place in the HAZ region next to the fusion line. In particular, the occurrence of the potentially detrimental δ-ferrite has not received attention yet. Little is known about the location of this phase, maximum volume fraction and mechanism of formation.

To see the effect of steel chemical composition on the presence of δ-ferrite, the present work focuses on two autogenously welded steels representing the extremes of the composition range currently marketed.

Materials composition

Steels A and B, whose chemical compositions are reported in table 1, cover the composition range of the low carbon “13 %Cr” martensitic stainless steels.

Steel A (UNS S41426), is designed for applications requiring some corrosion resistance in hydrogen sulfide media, and contains therefore a relatively large amount of molybdenum[3]. To ensure a complete austenitic microstructure at solution temperatures, large concentrations of nickel[4] are added.

Steel B is on the other hand a leaner alloy designed for use in slightly corrosive environments and therefore does not require addition of molybdenum.

Thermodynamic calculations

Phase diagrams

Low-carbon martensitic stainless steels are essentially alloys of Fe, Cr and Ni. Figure 1 shows that a pure Fe-13 %Cr binary alloy cannot be made fully austenitic at solution temperatures. Figure 2 shows the strong enlarging effect of nickel on the austenite stability field.

During cooling from the melt, low carbon martensitic stainless steels first solidify as δ-ferrite followed by austenite precipitation. Further cooling below the martensite-start temperature (Ms), leads to the transformation of austenite into martensite. The possible phases found in actual materials are therefore martensite, retained austenite and δ-ferrite but also carbo-nitrides such as Ti(C,N),

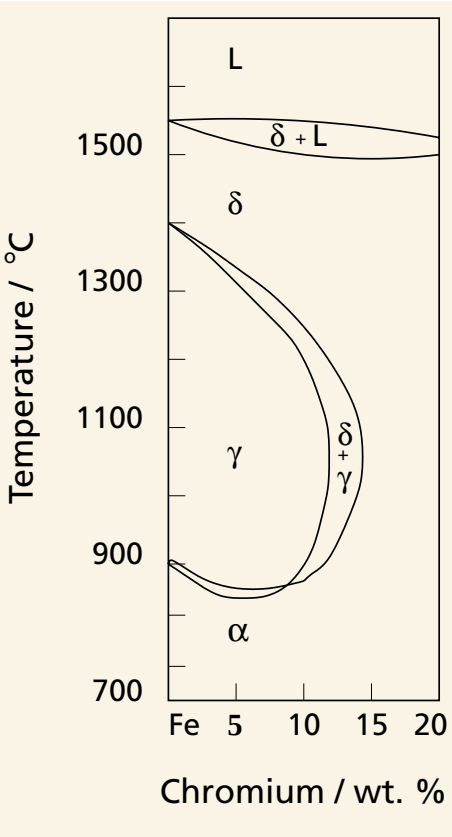

Figure 1: Fe-Cr phase diagram.

Steel	C	Si	Mn	Ni	Cr	Mo	Cu	Ti	N
A	0.01	0.26	0.46	6.46	12.2	2.48	0.03	0.09	0.0070
B	0.01	0.18	1.14	1.55	10.9	0.01	0.49	0.01	0.0006

Table 1: Chemical composition of steels A and B in wt %.

$M_{23}C_6$ and M_2X. However, the low level of carbon and nitrogen coupled with the high stability of Ti(C,N) means that precipitation of other carbo-nitrides is very limited [1].

Phase transformation temperatures

To understand the microstructures that develop in the high temperature HAZ of welded joints, it is useful to estimate the temperatures of the onset and completion of δ-ferrite formation (A_4 and A_5) as well as the melting temperature (Tm). To this end, thermodynamic calculations for the exact composition of the experimental steels have been carried out.

All calculations were performed using the MTDATA computer package. MTDATA developed by the National Physical Laboratory (NPL), is capable of performing detailed equilibrium and para-equilibrium calculations for a wide range of alloys. Experimentally determined parameters are used to model thermodynamic variables, for this reason the reliability of the calculations it performs depend on the parameter present in the database.

The program utilises an optimisation routine for minimising the Gibbs free energy of the system. As a result, phase transformation temperatures, phase stabilities and volume fractions can be predicted.

Considering the high temperatures at which δ-ferrite forms in carbon steels (~1400 ° C) it may be reasonable to assume that substitutional elements have time to redistribute during a weld thermal cycle. Thus, calculations were performed assuming equilibrium. As interest is based on the upper part of the phase diagram, austenite, ferrite and liquid were the only phases allowed for in the calculations. Silicon was not taken into account in the calculations as it has been reported to introduce inaccuracies in prediction for martensitic stainless steels [2].

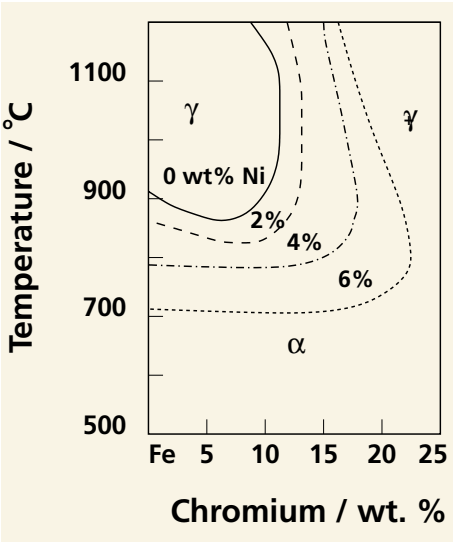

Figure 2: Effect of Ni on austenite stability field.

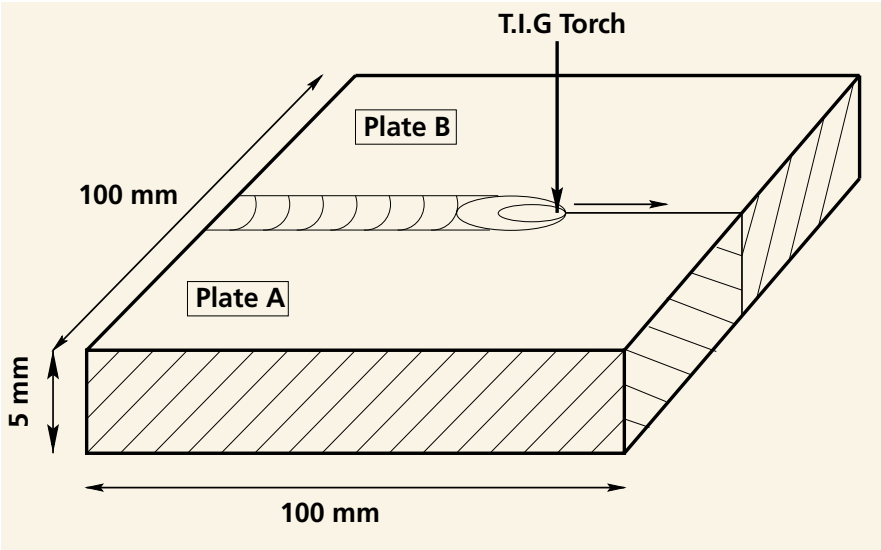

Figure 3: Schematic illustration of the welding operation.

Steel	Ae_4 (°C)	Ae_5 (°C)	Melting T. (°C)
A	1223	1403	1480
B	1255	1355	1488

Table 2: Calculated phase transformation temperatures performed on steels A and B.

Weld	Current	Voltage	Travel speed	Arc efficiency	Heat-input
	(A)	(V)	(mm s-1)	[2]	(kj mm^{-1})
WAB1	208	9.3	1.66	0.6	0.7

Table 3:Welding parameters for weld WAB1.

Results

The equilibrium temperatures of the onset and completion of δ-ferrite phase formation referred to as Ae_4 and Ae_5, along with the melting temperatures are reported in table 2.

Ferrite formation is predicted to be completed at temperatures above 1350ºC. Also, the temperature range of ferrite formation is predicted to vary between 180 and 100 ºC for steel A and B respectively. The temperature interval between Ae_5 and the melting temperature is seen to be greater for steel B (133 ºC) than A (77 ºC).

Experimental procedure

Welding

Plates of dimension 100µ50µ5 mm were machined out of seamless pipes taken parallel to the tube axis. An autogenous weld referred to as WAB1 was produced using an automated T.I.G. welding process. The heat-input was selected so as to avoid full penetration. For direct microstructural comparison, steels A and B were welded along the edge as illustrated on figure 3.

The welding conditions are summarised in table 3. Argon was used as shielding gas during the welding operation. After welding, the weld was naturally air-cooled. A transverse section was taken approximately in the middle of the weld for optical examination.

Optical microscopy

The microstructures were revealed by grinding and polishing the specimen to a 1 µm finish and by etching using either a modified Villela's reagent[5] or an electrolytic etchant based on sulphuric acid[6] at an applied potential difference of 3-4 V, or a color

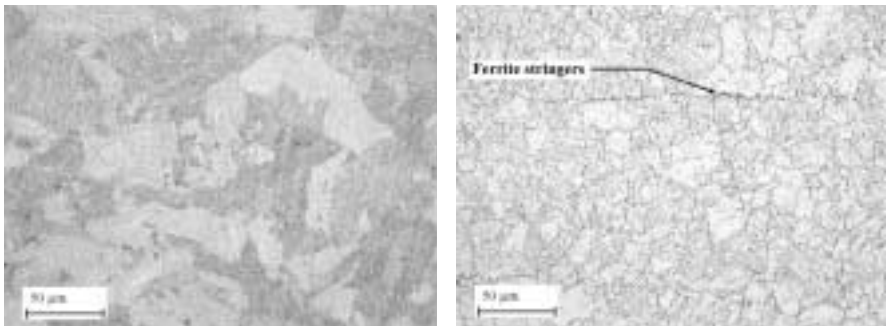

Figure 4: Initial microstructures of steels A (left) and B (right) etched with Villela's reagent.

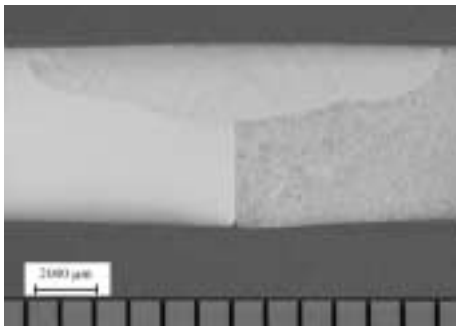

Figure 5: Macrophotograph of weld WAB1.

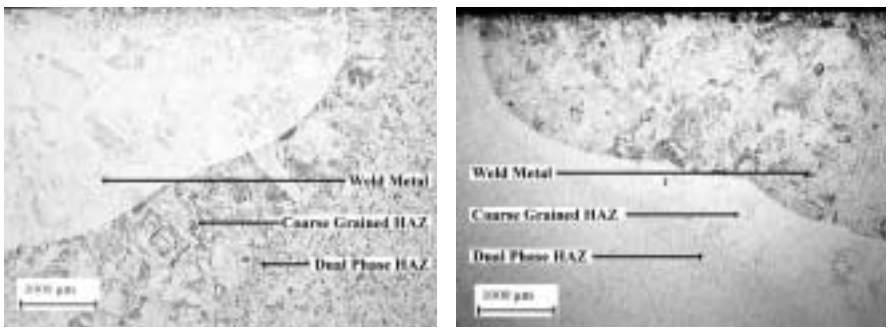

Figure 6: Microstructures of steel A (left) and B (right) in weld WAB1 etched with Villela's reagent.

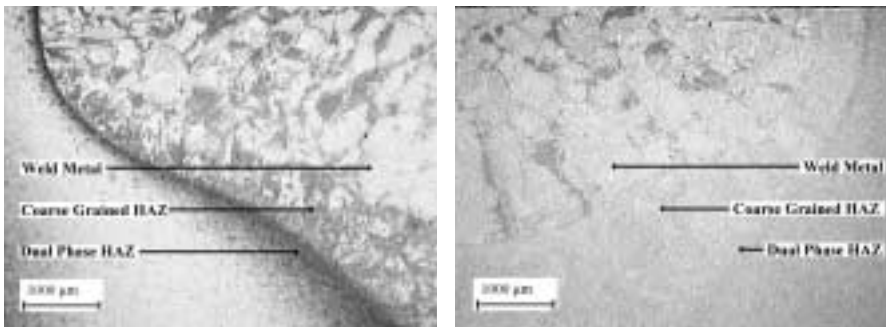

Figure 7: Microstructures of steel A (left) and B (right) in weld WAB1 electrolitically etched.

etchant[7]. Pictures were taken on a Leica DMR digital camera.

Image analysis

The volume percent of δ-ferrite at specific positions in the HAZ has been determined using an image analysis software. The extent of each HAZ region was obtained by measuring along lines parallel to the top surface on high magnification pictures.

EDX microanalysis

To examine potential partitioning of the alloying elements, some micro-analytical tests were carried out using an energy dispersive X-ray (EDX) analysis system on a CAMSCAN CS144 scanning electron microscope. ZAF corrections were employed and acquisition time was set to 100 seconds.

Results

As-received microstructures

The initial microstructures of the materials revealed with Villela's reagent are shown in figure 4. They consisted of tempered martensite with some occasional ferrite stringers in steel B.

Weld WAB1

A macrophotograph of the completed weld is shown in figure 5. The microstructures of weld WAB1 revealed with Villela's reagent and the electrolytic etchant are shown on figures 6 and 7 respectively.

The HT-HAZ microstructure from the fusion line consisted of a coarse-grained region followed by a region where both ferrite and martensite were present and finally an entirely martensitic region.

A single etchant was not able to reveal simultaneously all the details of the microstructure on either side of the weld. Villela's reagent clearly outlined both the former weld pool and grain coarsened region of the HAZ. The electrolytic etchant proved very effective in revealing both the details of the grain coarsened and dual phase regions.

Width of individual regions

The widths of the coarse-grained and dual phase HAZ were, on both steels, seen to increase from the top to the bottom surface of the plates. The volume percent of δ-ferrite, measured at the bottom of both plates, was larger for steel A (27 ± 5 %) than B (5 ± 1 %) as seen on figure 11.

Table 4 indicates, for each side of the weld, the maximum width of each region measured at the top surface and at the maximum weld pool penetration. At the maximum weld pool penetration (3.4 mm), the coarse grained region of steel B was about 60

Depth (mm)	CG-HAZ (µm)		DP-HAZ (µm)	
	Steel A	Steel B	Steel A	Steel B
0.0	450	530	130	80
3.4	3180	5400	1270	390

Table 4: Width of coarse-grained (CG) and dual phase (DP) HAZ measured at different depths.

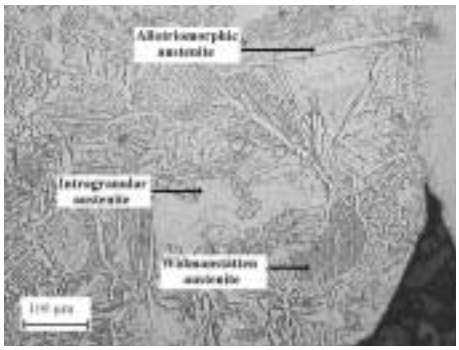

Figure 8: Details of the CG-HAZ of steel A, as seen at the bottom of the plate (electrolytically etched).

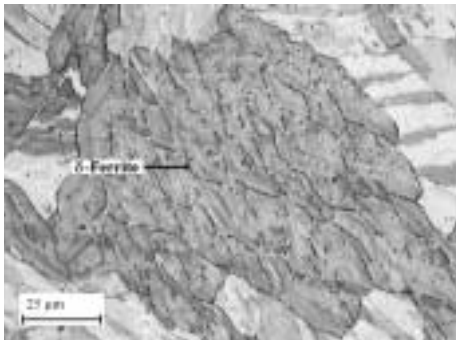

Figure 9: Ferrite trapped within the former Widmanstätten austenite in the CG-HAZ of steel A. Sample etched with color etchant.

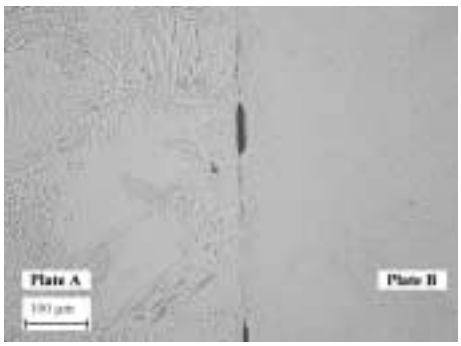

Figure 10: CG-HAZ comparison between steels A and B. (Electrolytically etched).

% wider than steel A. At the same depth, the width of the dual phase HAZ was about three times that of the HAZ of steel A.

Coarse-grained region

Steel A coarse-grained region had similar substructures as the weld metal. The prior δ-ferrite grains were composed of former allotriomorphic (localised at grain boundaries) intragranular and also Widmanstätten austenite (within the grains and at grain boundaries) as shown on figure 8. Very small amount of "lathy" δ-ferrite, whose width was about 400 nm, could be found within former Widmanstätten austenite laths as shown on figure 9.

Steel B did not show evidence of former Widmanstätten austenite structure in its coarse-grained HAZ compared to steel A (cf. figure 10).

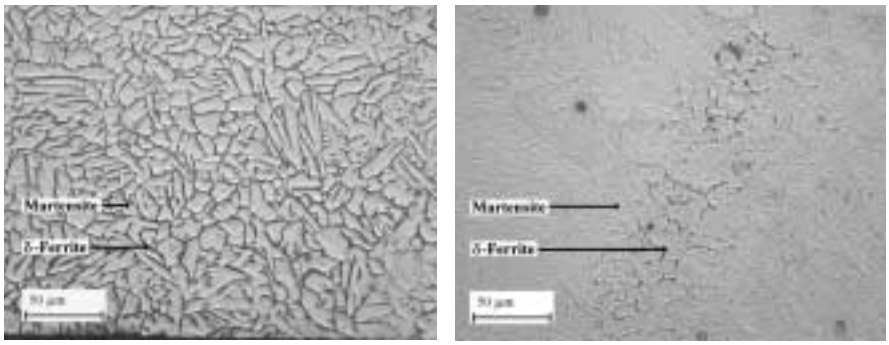

Figure 11: Details of δ-ferrite phase observed in the dual phase HAZ of steels A (left) and B (right).

Dual phase region

The dual phase HAZ on either side of the weld had a smaller grain size than the coarse-grained HAZ as seen on figure 11. No former Widmanstätten austenite could be found in the dual phase areas.

Five EDX microanalyses were performed both on the martensitic matrix and δ-ferrite at three different positions in the dual phase region, table 5 summarises the results.

Ferrite in the dual phase region of steel A was found to be significantly Cr and Mo enriched as well as Ni depleted. Similarly, ferrite in steel B (Mo free alloy), was found to be Cr enriched and Ni depleted.

Discussion

Weld geometry

The HAZ profile obtained in the weld performed in this study was not representative of the one of a real weld.

The shape of the weld was not hemispheric (i.e.: the high temperature isotherms in the transverse direction of the weld were not parallel to each other and semi-circular). The latter phenomenon is due to the relatively small thickness of the plates and the relatively large heat-input employed[3]. Under such conditions, the distance between high temperature isotherms increases from the top to the bottom surface and so does the width between the Ac_4-Ac_5 isotherms.

In the case of hemispheric welds, it would be possible to relate the peak temperature distribution in HAZ with the corresponding area experimentally observed in the HT-HAZ as shown on figure 12.

The obtained HAZ profile was however found very well suited to show that in some welding configuration, the volume percentage of δ-ferrite in HAZ can be relatively high (27 %).

Microstructure evolution in coarse-grained HAZ

Figure 13, shows the expected microstructural changes occurring in the coarse-grained HAZ of steel A. At the Ac_4 temperature, austenite starts to transform into δ-ferrite and the reaction is completed at the Ac_5 temperature. Once the δ-ferrite single-phase field has been reached, grain growth occurs. Upon cooling δ-ferrite decomposes into allotriomorphic, intragranular and Widmanstätten austenite. Below Ms the austenite transforms to martensite.

Phase	Steel A			Steel B		
	Cr	Ni	Mo	Cr	Ni	Mo
δ-ferrite	13.5 ± 0.9	4.8 ± 1.0	2.6 ± 0.4	13.2 ± 0.7	0.8 ± 0.3	-
Matrix	11.7 ± 0.3	7.0 ± 0.4	1.7 ± 0.2	10.6 ± 0.3	1.5 ± 0.2	-

Table 5: EDX microanalysis (wt %) of phases in steels A and B.

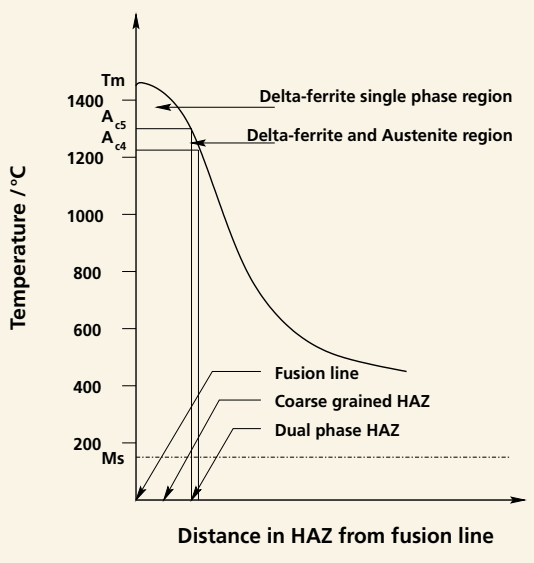

Figure 12: Schematic showing width of HAZ regions as a function of peak temperature distribution in HAZ.

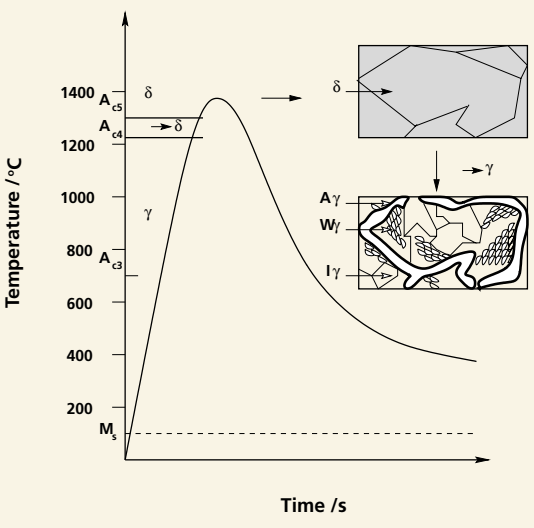

Figure 13: Schematic of steel A CG-HAZ microstructure evolution during welding.

In steel B, the decomposition of δ-ferrite into austenite did not reveal any substructure. The latter is consistent with the observation made on a range of austenitic stainless steels, that increasing the Cr/Ni ratio decreases the volume fraction of Widmanstätten austenite [4].

Widmanstätten austenite

The Widmanstätten austenite phase has (to the author's knowledge) never been reported before in both martensitic and low carbon martensitic stainless steels. Similar phase morphology has been encountered in austenitic stainless steels solidifying first as δ-ferrite [4,5,6].

Like Widmanstätten ferrite found in carbon steels, the appearance of Widmanstätten austenite is one of narrow wedges emanating either directly from a grain boundary, or from allotriomorphic ferrite (allotriomorphic austenite in the case of Widmanstätten austenite). This shape results from growth occurring along well defined planes, thus the plates align parallel with each other. Most authors agree that the Widmanstätten austenite structures originate by a diffusion-controlled transformation [4,7,8].

Coarse-grained HAZ width

Steel B coarse-grained HAZ was found to be larger than steel A. This is consistent with the larger predicted Tm-Ae_5 temperature.

Microstructure evolution in dual-phase HAZ

In the dual-phase region, the microstructural development can be summarised as follows (figure 14). During heating, growth of the δ-ferrite phase nucleated from prior austenite grain boundaries occurred towards the centre of the grains. Equilibrium dictates that ferrite stabilising elements (in particular Cr and Mo) partition into δ-ferrite. Upon cooling, back diffusion of Cr and Mo occur, but depending on the level of Cr and Mo enrichment, reverse transformation of the stabilised ferrite may not be complete. Hence, for a given Ni concentration, steels possessing lower concentration of Mo are expected to retain less δ-ferrite in their dual phase HAZ.

However, as ferrite was found in the dual phase HAZ of steel B, partitioning between Cr and Ni in ferrite is also important.

Dual phase HAZ width

The widths of the dual phase region were always found to be larger in steel A despite a smaller Ae_4-Ae_5 temperature interval predicted. But as the measured Cr enrichment and Ni depletion of the δ-ferrite phase was less pronounced for steel B, reverse transformation might have occurred in a larger extent in steel B.

Conclusions

The following conclusions can be drawn:

- Low carbon martensitic stainless steels containing molybdenum are more likely to retain grain boundaries δ-ferrite due to the ferrite stabilising effect of molybdenum.
- The level of ferrite encountered in HAZ of steel A did not exceed 27 % at the bottom of plate A. This value has to be regarded as unusual compared to ferrite level that could be found in traditional butt welds.

Further work is required to :

- Predict the level of HAZ ferrite retention in real welds.
- Assess the effect of low level of HAZ d-ferrite on both mechanical properties and corrosion resistance.

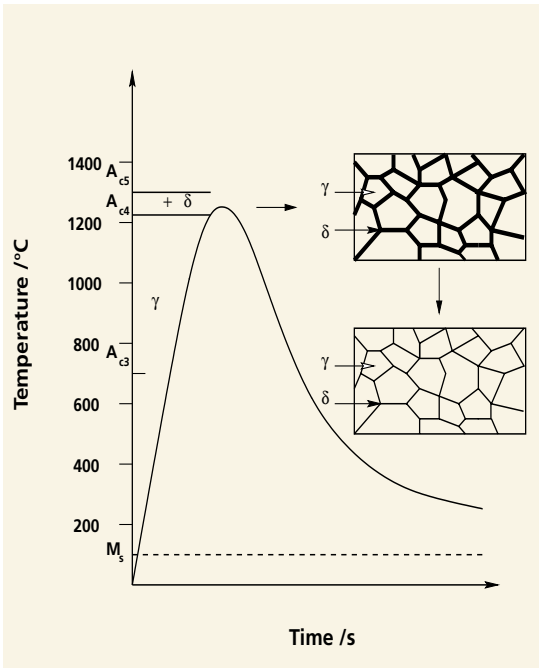

Figure 14: Schematic of the DP-HAZ microstructure evolution during welding.

References

[1] R. W. K. Honeycombe and H. K. D. H. Bhadeshia. Steels microstructures and properties. Edward Arnold, London, 1995.

[2] T. Cool and H. K. D. H. Bhadeshia. Austenite formation in 9Cr-1Mo type power plant steels. Science and Technology of Welding and Joining 2:36-42, 1997.

[3] O. Grong. Metallurgical Modelling of Welding. The Institute of Materials, London, 1994.

[4] G.L. Leone and H.W. Kerr. The Ferrite to Austenite Transformation in Stainless Steels. Weld. J. res. suppl., 61:13s-22s,1982.

[5] J. Singh, G.R. Purdy, and G.C. Weatherly. Microstructural and Microchemical Aspect of The Solid State Decomposition of Delta-ferrite in Austenitic Stainless Steels. Metallurgical Transactions,16A:1363-1369, 1985.

[6] T. Omura, T. Kushida, T. Hayashi, Y. Matsuhiro and Y. Komizo. Super 13 Cr Martensitic Stainless Steel Line Pipe by Super Laser Welding. In Supermartensitic Stainless Steels '99', pages 127-133, Belgium, 1999.

[7] J.C. Lippold and W.F. Savage. Solidification of Austenitic Stainless Steels Weldments Part I-a Proposed Mechanism. Weld. J. res. suppl., 58: 362s-374s, 1979.

[8] G. Blanc and R. Tricot. Solidification, Segregation et Homogeneisation des Aciers Inoxydables Austenitique Contenant de la Ferrite Delta. Mem. Sci. Rev. Met. 58: 735-753, 1979.

Notes

1. The HT-HAZ refers to the HAZ regions next to the fusion line.
2. Molybdenum containing alloys.
3. Strong ferrite stabilizer.
4. Strongest austenite stabilizer.
5. 1 gram of picric acid and 5 ml of HCl in ethanol.
6. Solution of 20 ml sulphuric acid with 0.1 g.l-1 ammonia thiocyanate in 80 ml distilled water.
7. 20 ml HCl 35 % in 80 ml distilled water and 1 gram of potassium metabisufite.

Acknowledgement

This paper was first presented at the Stainless Steel World America 2002 Conference and Expo.

About the authors

Dr Paul Woollin graduated from Cambridge University in 1984 and joined TWI in 1991. He is Senior Section Manager for Metallurgy and Corrosion at TWI and his primary areas of responsibility are research and development in the welding metallurgy and corrosion behaviour of stainless steels and failure investigations involving stainless steels. His current activities are concentrated on ferritic-austenitic and weldable 12%Cr stainless steels.

Dominique Carrouge is a PhD student working jointly with Dr Woollin at TWI and Professor Harry Bhadeshia of University of Cambridge.